

1 **GSK-3 knockout enhanced T cell proliferation and**
2 **glucose metabolism**

3
4 Author: Chen Liu

5 Supervisor: Prof. Christopher E Rudd

6 Département de microbiologie, infectiologie et immunologie, Faculté de médecine

7
8 **Keywords:** GSK-3; glucose metabolism; T cell activation; Immunotherapy.

9
10 **Abstract**

11
12 Glycogen synthase kinase-3 (GSK-3) is a multifaceted serine/threonine protein kinase.
13 In this study, we generated a conditional GSK-3 knockout (KO) mice, which only in
14 mature T cells. We noticed that KO T cells had a burst in differentiation followed by *in*
15 *vitro* activation with soluble anti-CD3 and anti-CD28. Based on the glucose
16 metabolism studies, KO T cells acquired elevated glycolysis capacity, as well as
17 OXPHOS in mitochondria. GSK-3 small molecule inhibitor treatment against mice B16
18 melanoma revealed that enhanced tumour clearance and cytotoxicity. The position of
19 GSK-3 in T cells remains unclear, further studies would be focused on fatty acid β-
20 oxidation (FAO) and the balance between FAO and glycolysis.

21
22 **Abbreviations**

23
24 APC: Antigen presenting cells

25 CTLA-4: Cytotoxic T lymphocyte associated protein 4

26 CD: Cluster of differentiation

27 DN: Double negative

28 ECAR: Extracellular acidification rate

29 ETC: Electron transport chain

30 GSK-3: Glycogen synthase kinase 3

31 MHC: Major histocompatibility complex

32 OCR: Oxygen consumption rate

33 OXPHOS: Oxidative phosphorylation

34 PD-1: Programmed cell death protein 1

35 ROS: Reactive oxygen species

36 SMI: Small molecule inhibitor

37 TCF-1: T cell factor 1

38 TIL: tumour-infiltrating lymphocytes

39 TME: Tumour microenvironment

40

41 **Introduction**

42

43 Great interests in tumour immunotherapy have been developed in the last decades,
44 approaches include preventing the activation of inhibitory checkpoints PD-1/L1 and
45 CTLA-4 (1); tumour-specific adoptive cell transfer (2) *etc.* Despite the success in
46 certain tumour types, resistance continuous to be an obstacle for immunotherapy.
47 Although full mechanism of immune resistance is yet to be clear, current evidence
48 suggests that resistance could due to insufficient tumour immunogenicity, irreversible
49 immune cell exhaustion, generation of an immunosuppressive tumour
50 microenvironment (TME) (3). T cell exhaustion is described as the dysfunction of T
51 cells, due to continuous exposure to antigen, sustained expression of
52 immunosuppressive receptors (e.g. PD-1, CD101) and maintained a transcriptional
53 state which is distinct from effector or memory T cells (4).

54

55 Upon antigen presentation from the antigen presenting cells (APC) by the MHC
56 molecule and co-stimulation molecules (CD80/86), naïve T cells activate a complex
57 network to initiate cell differentiation and proliferation. Cell signalling pathways
58 involved in this process include the wnt pathway, PI3K-Akt pathway, NF κ B pathway
59 and the NFAT pathway (5). T cell factor 1 (TCF-1) is a versatile transcription factor
60 which has multiple roles in T cell development, differentiation and exhaustion. In a
61 chronic infection episode, TCF-1 could preserve the functionality of cytotoxic T cells
62 by promoting the expression of effector-function related regulators such as EMOES
63 and downregulating the expression of PD-1 (6, 7). The glycogen synthase kinase 3
64 (GSK-3) is a serine/threonine protein kinase that has numerous substrates. GSK-3 was
65 originally discovered as a regulator in the glucose metabolism pathway, and now it has
66 been well-established to be a component within the wnt signalling pathway (8).
67 Previous studies have demonstrated that the inhibition of GSK-3 with could attenuates
68 T cell exhaustion by the downregulation of the expression of PD-1, thereby enhancing
69 T cell cytotoxicity for tumour clearance (9, 10). In the context of Wnt signalling
70 pathway, GSK-3 mediated phosphorylation triggers the destabilisation of β -catenin,
71 which in turn deactivate β -catenin and TCF-dependent gene expression (11). Function
72 normality of β -catenin is essential during T cell development (12). Absence of β -catenin
73 expression impaired the double negative (DN) -3 thymocytes to DN-4 thymocytes
74 transition (13). Intracellular dynamic of GSK-3 during cell division has been studied
75 (14). GSK-3 β phosphorylates cyclin D1 on Thr-286, which leads to the delocalisation
76 from the nuclear to the cytoplasm, during the S phase. In contrast, the *cyclin D1* gene
77 is a target of activated β -catenin, high level of β -catenin leads to constitutive high
78 upregulated cyclin D1 mRNA and protein level (15).

79

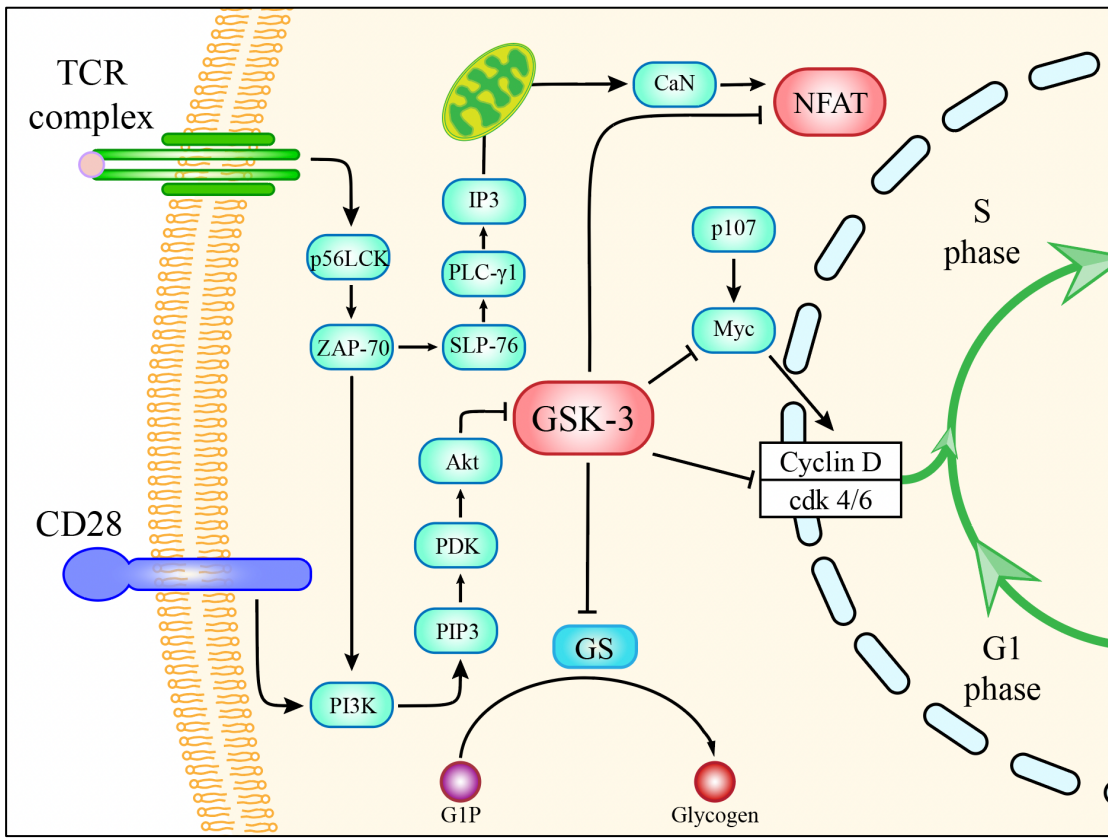
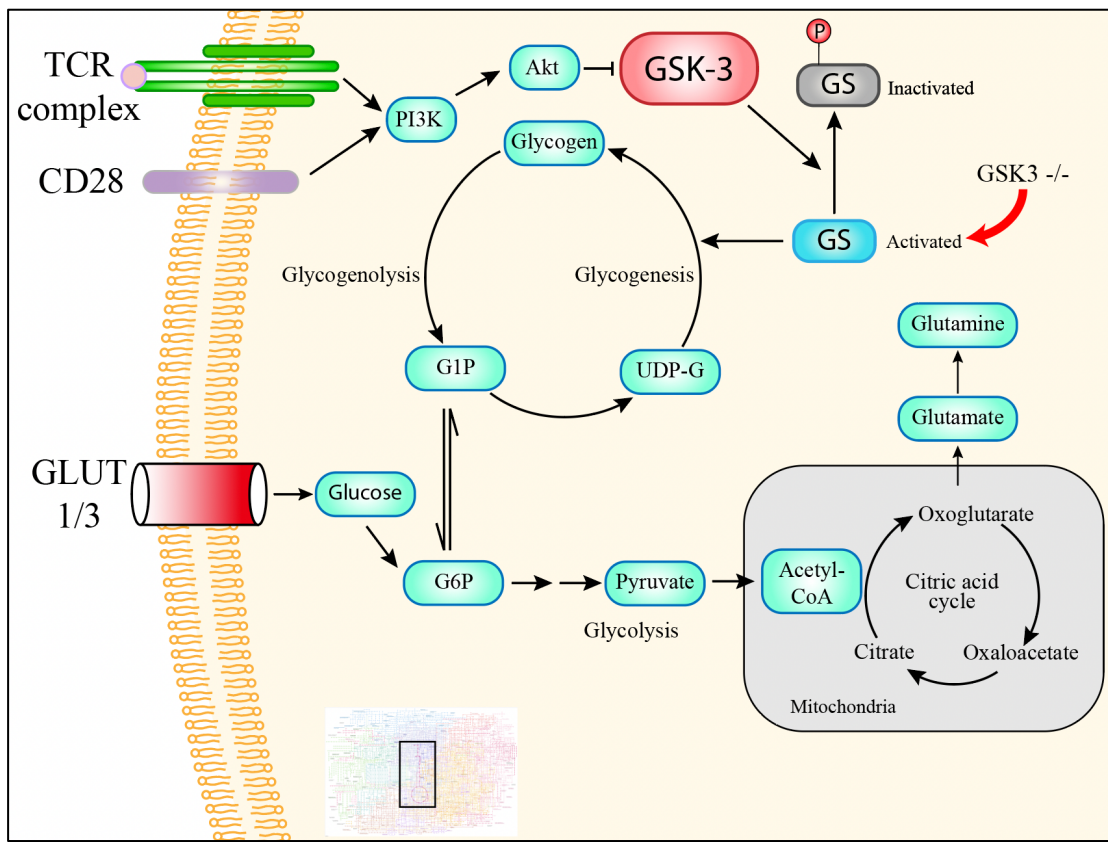


Figure 1. Schematic illustration of GSK-3 integrated in the TCR and CD28 signalling pathway and its effect on the progression of cell cycle.

Aerobic cellular respiration consists of two stages. The first step involves converting ubiquitously available biomolecules to fuel the mitochondria: remarked by the synthesis of pyruvate and acetyl-CoA entering the mitochondria. The second stage is where most of the ATP were synthesised: the citric acid cycle and the electron transport chain (ETC). All eukaryotes undergo glycolysis to fuel the mitochondria. Glycolysis is the process to break glucose down and produce pyruvate. Glycogenesis is the process to yield glycogen from glucose, in respond of elevated blood glucose level. GSK-3 phosphorylates glycogen synthase at three serine residues within the $-RYPRPASVPPSPSLSR-$ motif (16). However, unlike glycolysis, glycogenesis does not occur equally in all mammalian cell types. Essentially, liver and muscle cells are responsible for the massive production and destruction of glycogen. Other cell types may store glycogen at a lower level to fulfil a short-term energy requirement (17). *In vitro* experiments conducted on human astrocytes with insulin stimulation suggested that the increment in astrocytes proliferation is insulin dose-dependent (18). Although the authors did not find an increase in glucose-uptake, their results indicated that astrocytes are insulin-responsive and glycogen metabolism could alter cell proliferation. Knocking out GSK-3 in B cells has led to doubled glycolysis and OXPHOS capacity, and increased cell number (19). Such studies suggesting that glucose and glycogen metabolism could alter the proliferation in certain cell types, not only the hepatocytes or adipose tissue. However, it is unclear that how glucose metabolism could change the proliferation in T cells.



106
107 Figure 2. Function of GSK-3 in glycogenesis pathway and steps of glycolysis.
108 Overview of metabolism obtained from KEGG (20).
109

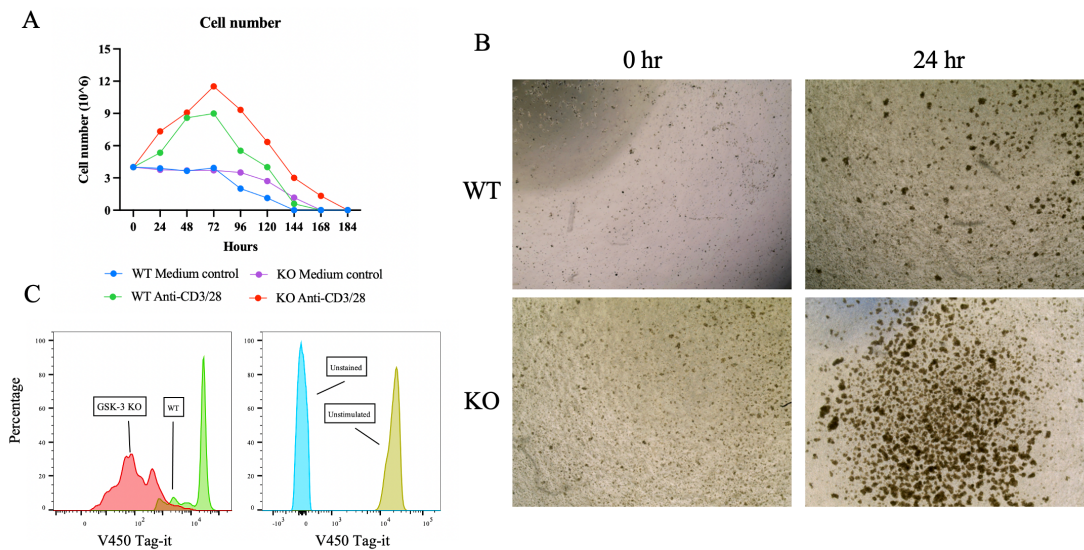
110 Numerous methods to inhibit GSK-3 have been developed. The use of lithium as a
111 GSK-3 inhibitor has more than 60 years of history (21). Lithium limits the activity of
112 GSK-3 by firstly, increasing its inhibitory-phosphorylation site (Ser9) and secondly, by
113 acting as a Mg^{2+} competitive inhibitor, who is required for GSK-3 to phosphorylate any
114 substrates (21). Due today, more than 40 types of pharmacological inhibitors against
115 GSK-3 have been created, most of them sit in the aminopyrimidine, anilinomaleimide,
116 pyrazolopyridazine or bisindolylmaleimide class (22). Completely block the expression
117 of GSK-3 seemed to be a more powerful method to inhibit GSK-3. However, GSK-3
118 knockout mouse embryo is not life-bearing and *in utero* deaths had been reported (23,
119 24). Thanks to the discovery of the lck distal promoter-cre (dLck-Cre) transgenic
120 system, gene of interest could be excised after thymocytes, therefore preventing any
121 deficiency in early immunity development (25). We generated conditional GSK-3
122 knock out (KO) mice based on this method, where GSK-3 is only knocked out in
123 splenocytes and mature T lymphocytes.

124
125 In this study, we compared the *in vitro* stimulation of the wild type (WT) and GSK-3
126 knock-out (KO) splenocytes, and their lifespan after activation. Glucose metabolism
127 were investigated, by using Seahorse-based glycolysis and mitochondrial assays and
128 glucose uptake assay. To study the *in vivo* effect of GSK-3, mice with B16 melanoma
129 were treated with GSK-3 small molecule inhibitor (SMI) and analysed the obtained
130 tumour infiltrating lymphocytes.
131
132

133 **Results**

134

135 GSK-3 knockout in T cells led to a proliferative burst at the first 24 hours of activation.
 136 Splenocytes were activated with soluble anti-CD3 and anti-CD28. A difference in cell
 137 number could be observed after 24 hours, which the GSK-3 KO (KO) T cells had a
 138 nearly doubled differentiation than wild type (WT) T cells. Cell numbers for both of
 139 the group reached a peak at 72 hours (day 3) (Figure 4A). Clustering is an indication of
 140 lymphocytes activity. In the KO group, larger and darker clusters have been observed
 141 (Figure 4B). Cells were stained with Tag-it stain to trace differentiation. After 24 hours
 142 of activation, the GSK-3 KO cells showed a higher degree of differentiation, where
 143 more peaks toward left were observed.



144

145 Figure 4. Proliferation of wild type (WT) and GSK-3 knockout (KO) T cells. A: Cell
 146 number for *in vitro* activation for 8 days; B: The formation of clusters which indicating
 147 proliferation; C: 24-hour Tag-it differentiation stain. Y-axis: Percentage, X-axis: Tag-
 148 it V450 fluorescence intensity.

149

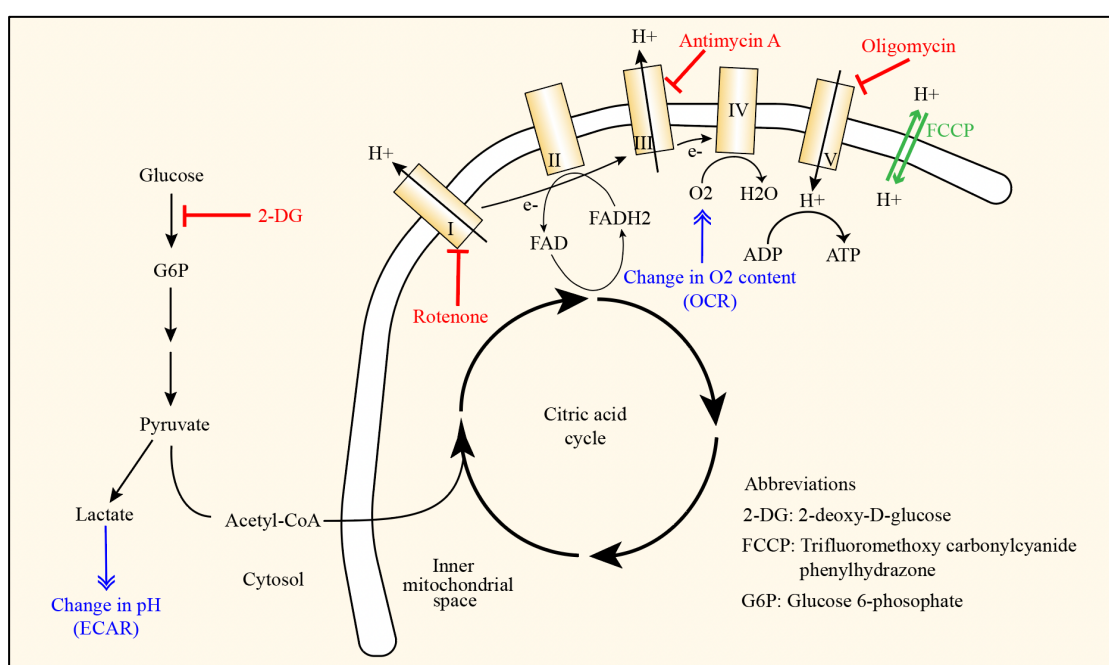
150 GSK-3 mediates the degradation of β -catenin. β -catenin is a key component of the
 151 canonical Wnt/ β -catenin pathway. β -catenin positively regulates the activity of Tcf-1
 152 (26). In absence of GSK-3, β -catenin accumulates within the cell and may help to
 153 explain why KO T cells has an advance during early activation phase.

154

155 As cell differentiation is a high energy-demanding procedure, we then investigated if
 156 there were any differences in cellular respiration between WT and GSK-3 KO T cells
 157 based on the Seahorse system. Glycolytic stress test and mitochondrial stress (mito-
 158 stress) test were performed. Figure 5 demonstrated the inhibitors and measurements of
 159 Seahorse assays. Glycolysis is the process for converting glucose to pyruvate and
 160 acetyl-CoA. The end-product of glycolysis pyruvate, could be converted to lactate,
 161 which could induce a change in the pH. In the glycolytic stress test, the Seahorse
 162 measures the ECAR to determine the rate and capability of glycolysis. Cells were
 163 placed in a glucose-free environment prior to the test. The injection of glucose allows
 164 cells to initiate glycolysis. Measurements done after first injection were the rate of
 165 glycolysis. The second injection is oligomycin. Oligomycin is a complex V (ATP
 166 synthase) inhibitor. Inhibition of complex V leads to a shut-down of mitochondrial ATP
 167 production, where cells solely rely on glycolysis to produce energy. This measures the

168 glycolytic capacity. The third injection, is 2-DG, which is a competitor of glucose. 2-
169 DG shuts down the glycolysis reaction. In this case, if any ECAR was measured, it
170 would be due to non-glycolytic processes.

171
172 In the mitochondrial stress (mito-stress) test, the oxygen consumption rate (OCR) was
173 measured. Prior to the addition of the first inhibitor oligomycin, the OCR reading
174 indicated the basal respiratory rate. When oligomycin was injected, OXPHOS
175 dramatically dropped as ATP synthesis was blocked. Proton leakage may still occur to
176 alter the oxygen level within mitochondria. The mechanism behind mitochondrial
177 proton leak in immune cells were poorly studied. It may has a function to protect cells
178 against ROS attack (27). FCCP induced a maximum OXPHOS rate. It allows the proton
179 to diffuse freely across the mitochondrial membrane. Rotenone (Rot) is a complex I
180 inhibitor, antimycin A (AA) is a complex III inhibitor. When cells were treated with
181 Rot/AA, proton trafficking was blocked and OXPHOS was therefore, shut down.
182



183
184 Figure 5. Seahorse measurements and reagents. Extracellular acidification rate (ECRA)
185 remarks the activity of glycolysis, oxygen consumption rate (OCR) indicates the
186 oxidative phosphorylation. (OXPHOS), which occurs within mitochondria.
187

188 T cells acquired enhanced glucose metabolism capacity as a result of GSK-3 knockout.
189 Glycolytic stress tests were performed to access the glycolysis rate and capacity of
190 CD3⁺ T cells. We found that the activated GSK-3 KO T cells did not show a
191 significantly increased real-time glycolytic rate, when compared to WT T cells. These
192 results consisted with our results from the glucose-uptake assay (Figure 6A, 6C).
193 Glucose enters the cytoplasm through Glut-1 or 3. No significant upregulation of Glut-
194 1 were observed between WT and GSK-3 KO T cells (Figure 6D). Upon T cell
195 activation, glut-1 were translocated to the cell membrane. This process is mediated
196 through the activation of the PI3K-Akt pathway (28).

197
198 Activated GSK-3 KO T cells had higher OXPHOS rate and capability. In absence of
199 GSK-3, T cells had higher basal respiration rate (Figure 6B). This corresponds with the
200 proliferative burst found in GSK-3 KO T cells, as cells requires more ATP for dividing.

201 Higher basal respiration rates in GSK-3 KO B cells were also found in Julia *et al*'s
202 study (19). The maximum respiration rate was doubled in GSK-3 T cells. The
203 difference between respiration capacity and basal respiration rate indicated the spare
204 capacity, which was reserved for acute energy demand. In a separate experiment, WT
205 and GSK-3 KO cells were cultivated in glucose-free medium (10% FBS), both groups
206 of cells could be activated and displayed normal morphology (figure not shown),
207 indicating T cell activation with solely soluble anti-CD3/28 could be achieved in a
208 relatively low glucose environment.

209

210 Combine these findings in glycolytic stress and mito-stress tests, GSK-3 restricted the
211 maximum glycolytic and OXPHOS capabilities, without detectable upregulating the
212 expression of Glut-1 or glucose uptake. However, the reason behind how GSK-3
213 knockout could increase T cell glycolytic capacity remains unknown. In conclusion, it
214 may suggest that GSK-3 limits the OXPHOS capacity in a glucose-independent manner.

215

216 In term of ATP production, although aerobic respiration (2 ATP per glucose molecule)
217 is a less efficient way than OXPHOS, it provides essential metabolic intermediates
218 which support OXPHOS, including G-6P, 3-PG, and acetyl-CoA (29). Glycolysis also
219 acts as a buffer system in balancing redox by indirectly promoting the synthesis of
220 NAD⁺/NADH (30). In results of elevated mitochondria activity, the addition of 2β-
221 mercaptoethanol (2-ME) in the culture medium is essential to maintain cellular viability.

222

223 In T cells, mitochondria is fueled by glycolysis and fatty-acid β-oxidation (FAO) (31).
224 The increase in OXPHOS may be due to an upregulated FAO rate. Therefore, we would
225 like to investigate the fatty acid storage and uptake in future experiments.

226

227 T cell immunity is linked to its metabolism. The activation of T cells is mediated by the
228 TCR-CD3 and CD28 costimulatory signalling. Once activated, T cells could survive in
229 a low glucose-viability environment (32). Glucose uptake is initiated as the results of
230 TCR-stimulated pathway, and enhanced by the CD28-PI3K-Akt axis (28). However,
231 our study did not demonstrate strong evidence that glucose uptake or Glut-1 expression
232 could be affected by the presence/absence of GSK-3. T cells with elevated glucose
233 metabolism showed an increased inhibitory phosphorylation of GSK-3, to protect cells
234 against apoptosis by reducing nuclear exportation of NFAT, and the stabilisation of mcl-
235 1 (33). As the PI3K-Akt signalling pathway promotes the inhibition of GSK-3, CD28
236 ligation may be crucial for elevating glucose metabolism.

237

238 To assess the effect of GSK-3 inhibition *in vivo*, we treated mice with B16 melanoma
239 cells with GSK-3 SMI (SB415286, SB). Mice were treated with either GSK-3 SMI or
240 PBS, as a control. Both groups survived for 6 does, 15 days after implantation. Necrosis
241 was an indication to terminate the study. Differences in tumour volumes became
242 significant on day 13, where GSK-3 SMI treated mice showed a lower tumour volume
243 than the control group (Figure 7B), as well as tumour mass (Figure 7C).

244

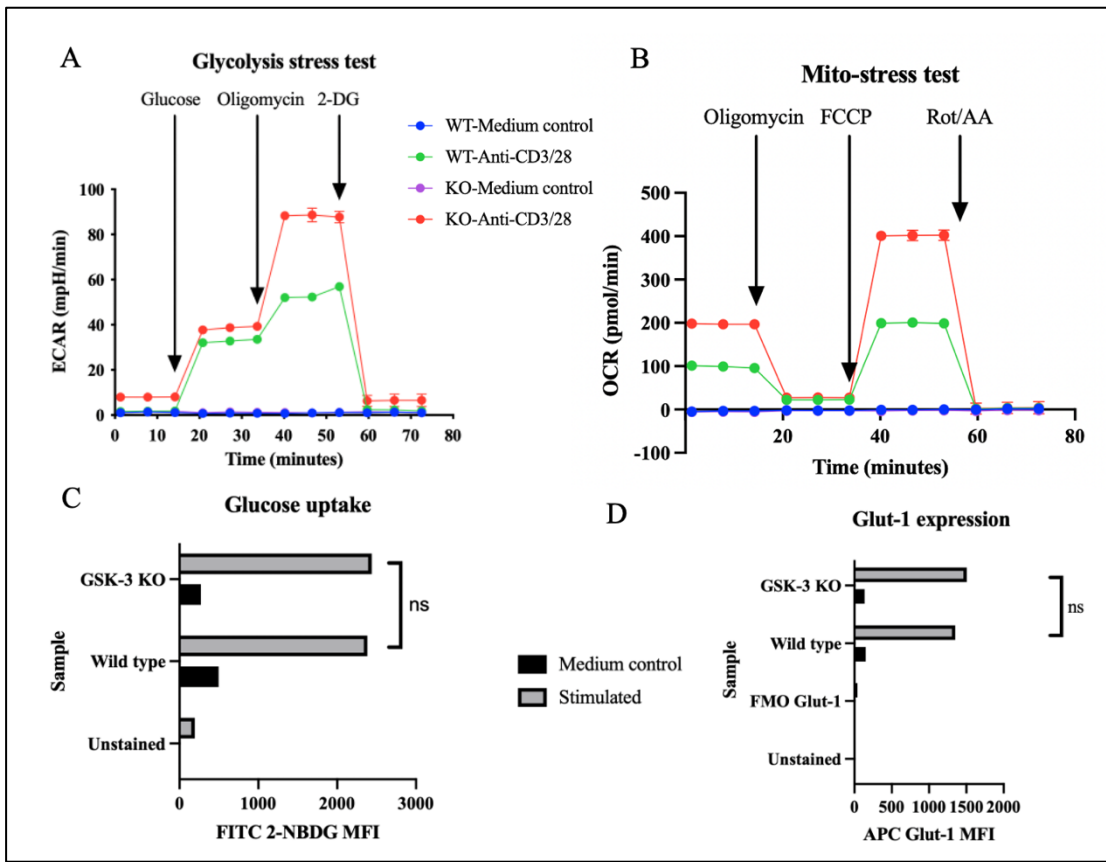


Figure 6. Seahorse glycolytic stress test (A) and mito-stress test (B). Glucose uptake (C) and Glut-1 surface expression (D) was measured.

245

246

247

248

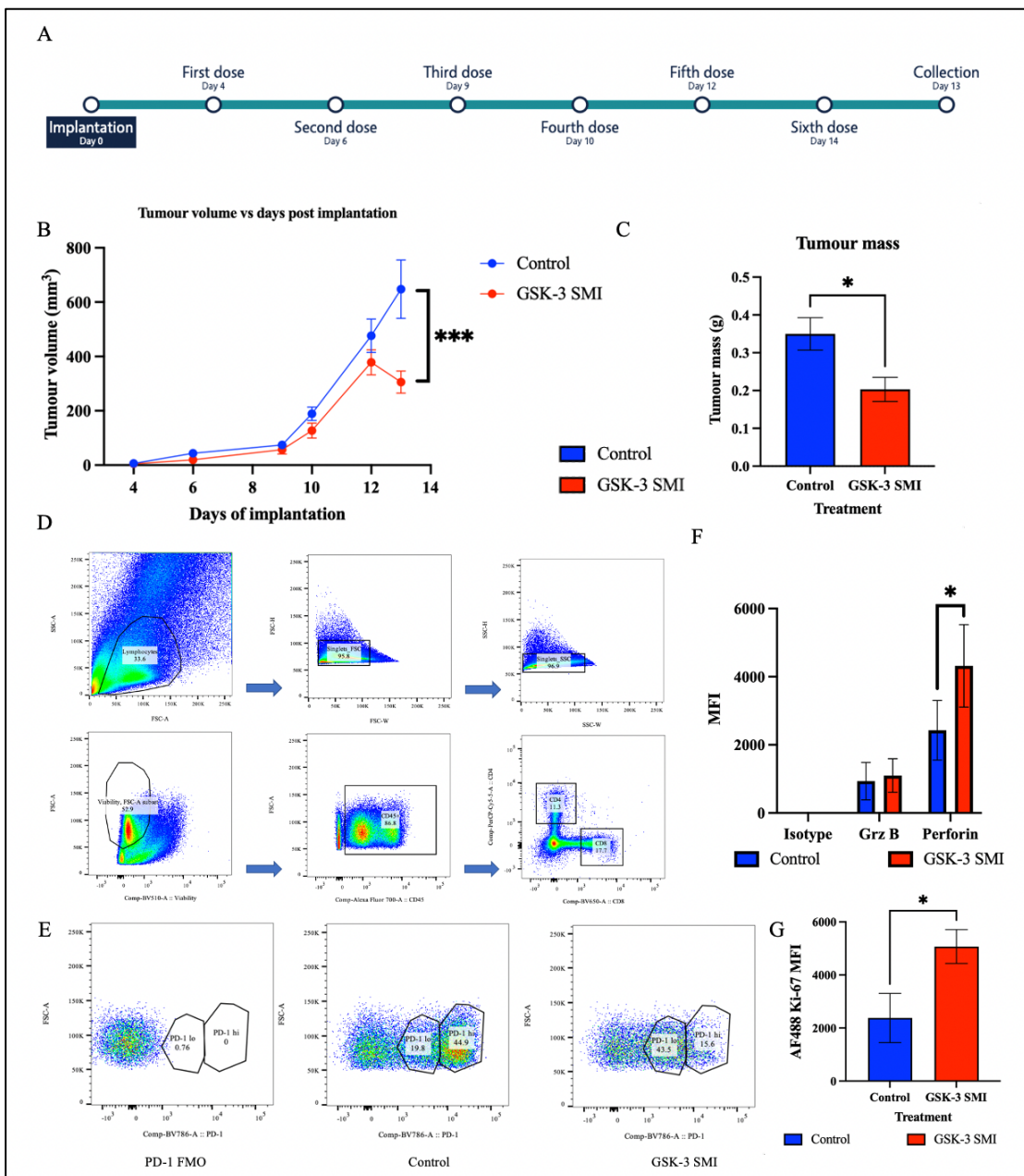
Tumour infiltrating lymphocytes (TILs) were separated and investigated by flow cytometry. We found after the GSK-3 SMI treatment, less PD-1^{hi} T cells were found in TILs (Figure 7E). Lower tumour mass and volume suggested higher tumour clearance. We access the cytotoxicity of CD8 T cells. We found higher perforin expression by TILs with GSK-3 SMI treatment (Figure 7F). The expression of Ki-67 in CD8 T cells was upregulated (Figure 7G) indicated prolonged proliferation.

255

256

Activation of immuno-checkpoints have the ability to reprogram cellular metabolism. PD-1 ligation could leads to deficiency in glycolysis and an increased rate of lipolysis of endogenous fatty acid and promote FAO (34). In contrast, TCLA-4 inhibits glycolysis without enhancing FAO (34).

260



261

Figure 7. GSK-3 SMI treatment against mice B16 melanoma. For control group, n = 7; treatment group, n = 9.

262

263

264

265

266

267

Methods

268

Animals

269

In this study, male C57BL/6J mice (Jackson Laboratory, USA) at 8-10 weeks old were selected as a wild type (WT) control. We generated a GSK-3 knockout (KO) mice by utilising the dLckCre recombinant system as described in the next section. Mice were euthanised and the spleens were harvested per sterile techniques. All *in vivo* experiments were compliant with the Hospital Maisonneuve-Rosemont Research Centre approved 2021-2516 B16F10 protocol.

270

271

272

273

274

275

276

Generation of the transgenic GSK3 dLckCre DLG mice

277
278 The GSK-3 knockout (KO) mice was generated by breeding between GSK3 $\alpha^{\text{flox/flox}}$
279 $\beta^{\text{flox/flox}}$ mice with B6.Cg-Tg(Lck-cre)3779Nik/J mice (Jackson Laboratory, USA).
280 GSK-3 flox expression was confirmed by PCR-based genotyping.
281

282 *Tumour implantation, monitoring and treatment*
283

284 B16F10 melanoma cells were trypsinated and washed with DMEM media. Cells were
285 resuspended to 8×10^6 cells/ml. Mice were shaved, anaesthetised, and received 0.5 ml
286 of cell suspension subcutaneously.
287

288 Tumour volume was monitored for every 2 two days, using the estimation of $volume =$
289 $length \times width^2$. Subcutaneous treatment with 400 mg/ml GSK-3 SMI SB415286 (SB41)
290 (Sigma, USA, S3567) in PBS began from day 4 post implantation. For every two days,
291 a new dose was given. All mice were euthanised on day 13, six doses were given each
292 mouse in total. PBS was given to the control group. Tumour mass was weighted after
293 removal from the animal.
294

295 *Tumour-infiltrating lymphocytes (TIL) separation*
296

297 Tumour tissue were harvested in to complete DME media. Tumour was chopped by a
298 blazer and incubated with TIL librase, DNase I at 37°C for 20 minutes. Cell suspension
299 were smashed, filtered through a 70 mm strainer, and washed with cold FACS buffer.
300 Cells were resuspended in 6 ml of FACS buffer and transferred to Ficoll-containing
301 tube. Cells were then spined at 21°C for 20 minutes at 2000 rpm, with minimum
302 acceleration or breaking. After the discontinuous gradients centrifugation, TILs were
303 separated from the middle layer, where tumour cells and other body tissues remains at
304 the bottom. TILs were carefully removed from Ficoll and washed with FACS buffer.
305

306 *Splenocytes isolation, in vitro cell activation and incubation*
307

308 Spleens were smashed and filtered with the 70 mm strainer and washed with culture
309 media. 1xRBC lysis was added to remove any remaining red blood cells. 10xRBC lysis
310 buffer was prepared with 4.01 g NH4Cl, 0.42 g NaHCO3, 0.185 g EDTA and top-up
311 with dH2O to 50 ml (35). In this study, RPMI 1640 (Corning, USA, 10-040-CV) were
312 supplemented with 10% FBS, 1% Pen/Strep (Corning, USA, 30-002-CI), 0.5% HEPAS
313 (Corning, USA, 25-060-CI) and 50 μM 2β-mercaptoethanol (Sigma, USA, 63689).
314 Cells were resuspended in this complete media at an initial concentration of 2×10^6
315 cells/ml on a 24-well plate. Final well concentration of 1 μg/ml soluble monoclonal anti-
316 CD3 (Bio X Cell, USA, 145-2C11) with/without anti-CD28 (Leinco, USA, C1658)
317 were utilised to activate T cells. Cells were incubated in a 37°C, 5% CO2 incubator for
318 at least 24 hours prior of any tests. Cells were counted every 24 hours with trypan blue.
319 Pictures of the cell culture were taken with the Evos XL Core Cell Imager
320 (ThermoFisher, USA, AMEX1100). For Seahorse metabolism assays, CD3+ T cells
321 were isolated with the Mouse CD3+ T Cell Enrichment Column (R&D Systems, USA,
322 MTCC-525). To maintain the growth condition, cell concentration was maintained at
323 2×10^6 cells/ml.
324

325 *Cell proliferation assay*
326

327 To monitor the differentiation of T cells, cells were incubated with 5 µM Tag-it Violet
328 Proliferation and Cell Tracking Dye (BioLegend, USA, 425101) at 37°C for 15 minutes
329 before activation. Cells were cultivated for 24 hours and measured by flow cytometry
330 at the V510 channel.

331

332 *Flow cytometry*

333

334 Cells were activated for at least 24 hours to analyse the surface and intracellular markers.
335 FACS buffer was reconstituted by adding 2% FBS in 1xPBS. Cells were washed with
336 1xPBS before viability staining. 45 minutes incubation on ice with the Fixable Viability
337 Dye F780 (Invitrogen, USA, 65-0865-14) was used to stain for viability. Cells were
338 washed with FACS buffer and ready for the 30 minutes surface staining. After surface
339 staining, cells were fixed with the Fixation solution (Invitrogen, USA, kit 00-5523-00)
340 for 45 minutes followed by 10 minutes permeabilization with the Permeabilisation
341 Solution (Invitrogen, USA, kit 00-5523-00) for 10 minutes. Incubate the cells with
342 antibody for 30 minutes on ice for intracellular staining. After this step, cells were
343 washed with FACS buffer twice and ready for measurement. To prepare compensation
344 samples, the UltraComp eBeads Compensation Beads (Invitrogen, USA, 01-2222-42)
345 were mixed with corresponding conjugated-antibody in FACS buffer, followed by a
346 10-minute incubation on ice. Antibodies were titrated to determine their optimised
347 concentration prior the staining procedure. Cells were well-mixed and kept in dark and
348 on ice before testing. Data were acquired from a BD LSRII Fortessa X-20 or BD
349 FACSCelesta (BD Bioscience, USA) flow cytometer.

350

351 *Cell gating*

352

353 Positive populations were determined by comparing with the fluorescence minus-one
354 (FMO), unstained or isotype samples. The table below stated all the surface and
355 intracellular antibodies being used in this study.

356

357 Table 1. Surface and intracellular markers for immune cell phenotyping

Target	Fluorochrome	Manufacturer	Clone/Cat no.
CD3ε	AF700	BD Bioscience	500A2
CD4	PerCp/Cy5.5	Biolegend	RM4-4
CD8α	BV650	Biolegend	53-6.7
TCRβ	BUV395	BD Bioscience	H57-597
PD-1	BV786	Biolegend	29F.1A12
CD44	PerCp/Cy5.5	Biolegend	IM7
CD127	BV421	Biolegend	A7R34
KLRG-1	PE	Biolegend	2F1
Tim-3	PE	BD Bioscience	5D12/TIM-3
TCF-1	AF647	Cell signalling	C63D9
β-catenin	AF488	Invitrogen	15B8
Cyclin D3	PE	Biolegend	DCS-22
Ki-67	PE-Cy7	Biolegend	16A8
Glut-1	APC	Abcam	EPR3915
Viability	APC-eF780	Invitrogen	65-0865-14

358
359 Before identifying any cell subsets, viable cells were selected according to this route
360 (Figure 7D): *Lymphocytes -> Singlets (FSC & SSC) -> Viable cells.*
361 Effector cells: $CD8^+ TCR\beta^+$ -> $CD44^+$ -> $CD127^{lo} KLRG-1^{lo}$
362 Memory precursor effector cell: $CD8^+ TCR\beta^+$ -> $CD44^+$ -> $CD127^{hi} KLRG-1^{lo}$
363 Short-lived effector cell: $CD8^+ TCR\beta^+$ -> $CD44^+$ -> $CD127^{lo} KLRG-1^{hi}$
364

365 *Metabolism study*

366

367 Cell maximum oxygen consumption rate (OCR) and extracellular acidification rate
368 (ECAR) were measured by mito-stress test (Agilent, USA, 103015-100) and glycolysis
369 stress test (Agilent, USA, 103020-100) respectively, based on the Seahorse XFe96
370 analyser (Agilent, USA, 101991-100). On day 0, $CD3^+$ T cells were activated and
371 incubated. 10 μ L of 50 μ g/ml poly-D lysin (PDL) (Gibco, USA, A3890401) were added
372 to coat the Agilent 96-well plate and put in 4°C overnight. On the proceeding day, PDL
373 coating plate was washed with dH₂O and air-dried with the cover opening. To calibrate
374 the Seahorse cartridge, 200 μ L of Seahorse XF Calibrant (Agilent, USA, 100840-000)
375 were added to each well and put into a non-CO₂ incubator for 45 minutes. T cells were
376 resuspended in complete Seahorse XF RPMI media (Agilent, USA, 103681-100) with
377 200 mM L-glutamine (Sigma, USA, 59202C), 25 mM D-glucose (Sigma, USA, G8644)
378 and 2 mM sodium pyruvate (Sigma, USA, S8636) and transferred to the PDL coated
379 96-well plate. Before tests commenced, cells were put in the non-CO₂ incubator for 1
380 hour to suppress mitochondrial respiration. Inhibitors were prepared as per
381 manufacturer's instruction.

382

383 Flow cytometric measurement of glucose uptake was based on the detection of the
384 fluorescent D-glucose analogue 2-[*N*-(7-nitrobenz-2-oxa-1,3-diazol-4-yl)-amino]-2-
385 deoxy-D-glucose (2-NBDG) (36) (Invitrogen, USA, N13195). Cells being activated for
386 24 hours were collected, washed and resuspended in glucose-free RPMI medium
387 (Corning, USA, 10-043-CV). Cells were incubated with 30 μ M 2-NBDG for 1 hour,
388 and washed with PBS for two times for surface and intracellular staining.

389

390 *Software and statistical analysis*

391

392 All experiments were repeated at least three times. FlowJo 10 (BD, USA) was used to
393 process the flow cytometry data. Results of the Seahorse metabolism assay were
394 analysed with the Seahorse Wave Desktop Software 2.6 (Agilent, USA). All other data
395 analysis and visualisation, unless specified, were achieved by Prism 9 (GraphPad,
396 USA). In a Mann-Whitney test, $p = 0.05$ was used as a threshold for signficancy.
397 Pathway illustrations were made with Adobe Illustrator 2022 (Adobe, USA).

398

399 **Conclusion**

400

401 GSK-3 is more than a namesake. In conclusion, our present study provided an insight
402 on the role of GSK-3 in glucose metabolism in T cells. The knockout of GSK-3 in T
403 cells promotes cell differentiation, glycolytic and OXPHOS capacity, likely in a
404 glucose-independent mechanism. The *in vivo* treatment of mice B16 melanoma with
405 GSK-3 SMI reduced the number of PD-1^{hi} TILs and enhanced tumour clearance. These
406 findings opened a new direction for connecting T cell metabolism and exhaustion.

407 Further studies in FAO would be valuable to reveal the effect of GSK-3 in the larger
408 picture of cellular metabolism.

409

410 Acknowledgement

411

412 This study cannot be achieved without the supports from Professor Christopher E Rudd
413 and all the lab members. Specifically, I would like to appreciate the following person:
414 Dr. Thai Hien Tu for providing guidance in the *in vivo* experiment, metabolism studies
415 including the Seahorse and glucose uptake assay; and Dr. Yunfeng Gao for generating
416 the GSK-3 dLckCre KO mice, management their breeding and the genotyping of the
417 individual offspring.

418

419 Reference

420

- 421 1. Wei SC, Levine JH, Cogdill AP, Zhao Y, Anang N-AAS, Andrews MC, et al. Distinct Cellular Mechanisms Underlie Anti-CTLA-4 and Anti-PD-1 Checkpoint Blockade. *Cell*. 2017;170(6):1120-33.e17.
- 422 2. June CH, O'Connor RS, Kawalekar OU, Ghassemi S, Milone MC. CAR T cell immunotherapy for human cancer. *Science*. 2018;359(6382):1361-5.
- 423 3. Lei Q, Wang D, Sun K, Wang L, Zhang Y. Resistance Mechanisms of Anti-PD1/PDL1 Therapy in Solid Tumors. *Front Cell Dev Biol*. 8:672.
- 424 4. Wherry EJ. T cell exhaustion. *Nature Immunology*. 2011;12(6):492-9.
- 425 5. Smith-Garvin JE, Koretzky GA, Jordan MS. T Cell Activation. *Annual Review of Immunology*. 2009;27(1):591-619.
- 426 6. Miller BC, Sen DR, Al Abosy R, Bi K, Virkud YV, LaFleur MW, et al. Subsets of exhausted CD8+ T cells differentially mediate tumor control and respond to checkpoint blockade. *Nature Immunology*. 2019;20(3):326-36.
- 427 7. Wang Y, Hu J, Li Y, Xiao M, Wang H, Tian Q, et al. The Transcription Factor TCF1 Preserves the Effector Function of Exhau sted CD8 T Cells During Chronic Viral Infection. *Front Immunol*. 10:169.
- 428 8. FRAME S, COHEN P. GSK3 takes centre stage more than 20 years after its discovery. *Biochemical Journal*. 2001;359(1):1-16.
- 429 9. Krueger J, Rudd CE, Taylor A. Glycogen synthase 3 (GSK-3) regulation of PD-1 expression and and its therapeutic implications. *Seminars in Immunology*. 2019;42:101295.
- 430 10. Taylor A, Rothstein D, Rudd CE. Small-Molecule Inhibition of PD-1 Transcription Is an Effective Alternative to Antibody Blockade in Cancer Therapy. *Cancer Research*. 2018;78(3):706-17.
- 431 11. Wu D, Pan W. GSK3: a multifaceted kinase in Wnt signaling. *Trends in Biochemical Sciences*. 2010;35(3):161-8.
- 432 12. Ma J, Wang R, Fang X, Sun Z. β -Catenin/TCF-1 Pathway in T Cell Development and Differentiation. *Journal of Neuroimmune Pharmacology*. 2012;7(4):750-62.
- 433 13. Xu Y, Banerjee D, Huelsken J, Birchmeier W, Sen JM. Deletion of β -catenin impairs T cell development. *Nature Immunology*. 2003;4(12):1177-82.
- 434 14. Diehl JA, Cheng M, Roussel MF, Sherr CJ. Glycogen synthase kinase-3beta regulates cyclin D1 proteolysis and sub cellular localization. *Genes Dev*. 12(22):3499-511.
- 435 15. Tetsu O, McCormick F. β -Catenin regulates expression of cyclin D1 in colon carcinoma cells. *Nature*. 1999;398(6726):422-6.

- 457 16. RYLATT DB, AITKEN A, BILHAM T, CONDON GD, EMBI N, COHEN P.
458 Glycogen Synthase from Rabbit Skeletal Muscle. European Journal of Biochemistry.
459 1980;107(2):529-37.
- 460 17. Lee W-C, Guntur AR, Long F, Rosen CJ. Energy Metabolism of the Osteoblast:
461 Implications for Osteoporosis. Endocrine Reviews. 2017;38(3):255-66.
- 462 18. Heni M, Hennige AM, Peter A, Siegel-Axel D, Ordelheide A-M, Krebs N, et al.
463 Insulin Promotes Glycogen Storage and Cell Proliferation in Primary Human
464 Astrocytes. PLOS ONE. 2011;6(6):e21594.
- 465 19. Jellusova J, Cato MH, Apgar JR, Ramezani-Rad P, Leung CR, Chen C, et al.
466 Gsk3 is a metabolic checkpoint regulator in B cells. Nature Immunology.
467 2017;18(3):303-12.
- 468 20. Kanehisa M, Furumichi M, Sato Y, Ishiguro-Watanabe M, Tanabe M. KEGG:
469 integrating viruses and cellular organisms. Nucleic Acids Res.49(D1):D545-D51.
- 470 21. Jope RS. Lithium and GSK-3: one inhibitor, two inhibitory actions, multiple
471 outcomes. Trends in Pharmacological Sciences. 2003;24(9):441-3.
- 472 22. Meijer L, Flajolet M, Greengard P. Pharmacological inhibitors of glycogen
473 synthase kinase 3. Trends in Pharmacological Sciences. 2004;25(9):471-80.
- 474 23. Kotliarov S, Pastorino S, Kovell LC, Kotliarov Y, Song H, Zhang W, et al.
475 Glycogen Synthase Kinase-3 Inhibition Induces Glioma Cell Death through c-MYC,
476 Nuclear Factor- κ B, and Glucose Regulation. Cancer Research. 2008;68(16):6643-51.
- 477 24. Monteiro da Rocha A, Ding J, Slawny N, Wolf AM, Smith GD. Loss of
478 Glycogen Synthase Kinase 3 Isoforms During Murine Oocyte Growth Induces
479 Offspring Cardiac Dysfunction1. Biology of Reproduction. 2015;92(5):127, 1-12.
- 480 25. Hennet T, Hagen FK, Tabak LA, Marth JD. T-cell-specific deletion of a
481 polypeptide N-acetylgalactosaminyl-transferase gene by site-directed recombination.
482 Proceedings of the National Academy of Sciences. 1995;92(26):12070-4.
- 483 26. Gattinoni L, Ji Y, Restifo NP. Wnt/ β -Catenin Signaling in T-Cell Immunity and
484 Cancer Immunotherapy. Clinical Cancer Research. 2010;16(19):4695-701.
- 485 27. Divakaruni AS, Brand MD. The Regulation and Physiology of Mitochondrial
486 Proton Leak. Physiology. 2011;26(3):192-205.
- 487 28. Palmer CS, Ostrowski M, Balderson B, Christian N, Crowe SM. Glucose
488 metabolism regulates T cell activation, differentiation, and f unctions. Front
489 Immunol.6:1.
- 490 29. Cascone T, McKenzie JA, Mbofung RM, Punt S, Wang Z, Xu C, et al. Increased
491 Tumor Glycolysis Characterizes Immune Resistance to Adoptive T Cell Therapy. Cell
492 Metabolism. 2018;27(5):977-87.e4.
- 493 30. NAD(H) and NADP(H) Redox Couples and Cellular Energy Metabolism.
494 Antioxidants & Redox Signaling. 2018;28(3):251-72.
- 495 31. Geltink RIK, Kyle RL, Pearce EL. Unraveling the Complex Interplay Between
496 T Cell Metabolism and Function. Annual Review of Immunology. 2018;36(1):461-88.
- 497 32. Jacobs SR, Herman CE, MacIver NJ, Wofford JA, Wieman HL, Hammen JJ, et
498 al. Glucose Uptake Is Limiting in T Cell Activation and Requires CD28-Mediated Akt-
499 Dependent and Independent Pathways. The Journal of Immunology.
500 2008;180(7):4476-86.
- 501 33. Macian F. NFAT proteins: key regulators of T-cell development and function.
502 Nat Rev Immunol. 2005;5(6):472-84.
- 503 34. Patsoukis N, Bardhan K, Chatterjee P, Sari D, Liu B, Bell LN, et al. PD-1 alters
504 T-cell metabolic reprogramming by inhibiting glycolysis and promoting lipolysis and
505 fatty acid oxidation. Nature Communications. 2015;6(1):6692.

- 506 35. Liu X, Quan N. Immune Cell Isolation from Mouse Femur Bone Marrow. Bio-
507 protocol. 2015;5(20):e1631.
- 508 36. Zou C, Wang Y, Shen Z. 2-NBDG as a fluorescent indicator for direct glucose
509 uptake measurement. Journal of Biochemical and Biophysical Methods.
510 2005;64(3):207-15.
- 511